

Phase transitions in a quasi-two-dimensional XY random magnetic system

K. Katsumata

*The Institute of Physical and Chemical Research (RIKEN), Wako, Saitama 351-01, Japan
and Research Institute of Applied Electricity, Hokkaido University, Sapporo 060, Japan*

J. Tuchendler

Laboratoire de Dispositifs Infrarouge, Université Paris VI, 4, Place Jussieu, 75230 Paris Cedex 05, France

Y. J. Uemura

Brookhaven National Laboratory, Upton, New York 11973

H. Yoshizawa

Institute for Solid State Physics, University of Tokyo, Roppongi, Minato-ku, Tokyo 106, Japan

(Received 8 June 1987)

The phase transitions of a randomly mixed quasi-two-dimensional antiferromagnet and ferromagnet $\text{Rb}_2\text{Mn}_{1-x}\text{Cr}_x\text{Cl}_4$ have been studied experimentally using ac susceptibility (χ), magnetization, and neutron scattering techniques. A characterization of the single crystals of $\text{Rb}_2\text{Mn}_{1-x}\text{Cr}_x\text{Cl}_4$ grown for this study is made with ac χ and electron-spin-resonance measurements. It turns out that the mixed system is a typical example of an XY magnet in the concentration range $0.1 \leq x < 1.0$. The concentration versus transition-temperature (x - T) phase diagram of this alloy under zero external magnetic field is constructed. The transition temperature from the paramagnetic (PM) to the antiferromagnetic phase decreases rapidly with increasing Cr concentration. A transition from the PM phase to the spin-glass (SG) phase is observed in the concentration region $0.34 \leq x < 0.5$. The mixed crystals with the concentrations $0.50 \leq x < 1.0$ show a reentrant spin-glass (RSG) transition; a sequence of transitions from the PM to ferromagnetic (FM) phase and from the FM phase to SG at a lower temperature. Qualitatively, the x - T phase diagram of $\text{Rb}_2\text{Mn}_{1-x}\text{Cr}_x\text{Cl}_4$ is explained by the theories on competing exchange interactions. The RSG transition is discussed in the context of recent theories on the two-dimensional XY spin glass.

I. INTRODUCTION

Extensive studies have been done on spin glasses (SG) in the last decade. One of the most interesting problems in this field has been whether an equilibrium phase transition does exist in SG or not. Various kinds of SG materials have been reported that are characterized with ac susceptibility (appearance of a cusp at the freezing temperature, T_{SG}) and/or magnetization (presence of a remanence below T_{SG}) measurements. Among them are dilute alloys where the long-ranged Ruderman-Kittel-Kasuya-Yosida (RKKY) interaction dominates, and insulators in which the interactions are predominantly short ranged. In recent years a considerable progress has been achieved in the theory of SG. Bray *et al.*¹ showed a possibility of a marginal transition at a nonzero temperature in the RKKY SG. For three-dimensional (3D) short-ranged Ising SG the Monte Carlo simulations^{2,3} strongly suggest that a phase transition takes place. In two dimensions, Morgenstern and Binder⁴ had already shown that there is no phase transition in the short-ranged Ising SG. In the case of short-ranged Heisenberg SG systems, the theories⁵ seem to be unfavorable to the existence of a phase transition at a finite temperature. Whether a phase transition does exist or not in short-ranged XY SG systems is still controversial. Let us consider what happens when a frustra-

tion⁶ is introduced into a two-dimensional (2D) XY system. As shown in Fig. 1(a), if there is an even number of antiferromagnetic bonds in the plaquette no frustration occurs. On the other hand, if there is an odd number of antiferromagnetic bonds the spins are canted⁷ due to the frustration effect [Figs. 1(b) and 1(c)]. The ground states of the two canted spin configurations have the same energy and thus are degenerated. Villain⁷ introduced the concept of chirality (κ) to characterize the spin states in Figs. 1(b) and 1(c) in such a way that the former has $\kappa = +1$ and the latter $\kappa = -1$. Kawamura and Tanemura⁸ have made a Monte Carlo study on a 2D XY SG and showed a possibility of a phase transition from the paramagnetic to chiral SG phase in the case when the numbers of ferromagnetic and antiferromagnetic bonds are equal. They also made a Monte Carlo study⁹ on the same system in the region rich in ferromagnetic bonds and found reentrance phenomena; with lowering temperature a transition from the paramagnetic (PM) to ferromagnetic (FM) phase takes place followed by an FM to SG transition. Experimentally, reentrant spin-glass (RSG) transition is signaled by a sudden decrease of magnetization around the RSG transition temperature. According to the study by Kawamura and Tanemura, the RSG state with low net magnetization in the 2D XY random magnet is a metastable one. A true equilibrium state in the system is very similar to the one seen in fer-

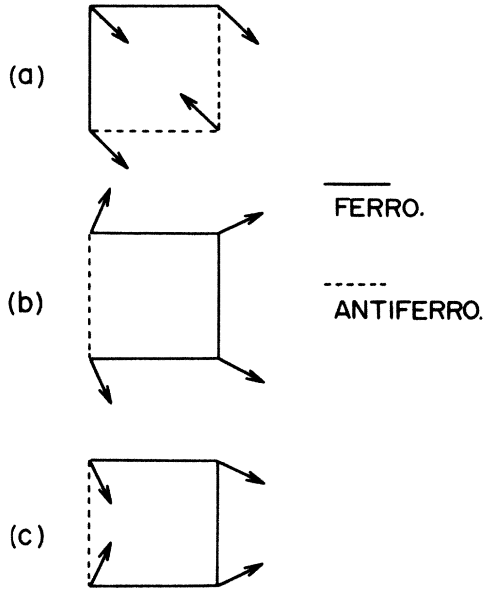


FIG. 1. The classical ground-state spin configuration of a set of four spins. The solid lines represent ferromagnetic exchange interaction and the dotted lines antiferromagnetic interaction. (a) Nonfrustrated plaquette; (b) frustrated plaquette with chirality (κ) = +1; (c) frustrated plaquette with κ = -1.

romagnets. Physically, this is explained as follows: when the sample is quenched from high temperature to RSG state, there are regions in which pairs of chiralities with the same sign (+ + or - -) are formed. These pairs disturb the surrounding spins seriously and make a vortex. This results in a state with low net magnetization. The metastable state has a higher energy than the ferromagnet like state. On the other hand, Jain and Young,¹⁰ who also performed Monte Carlo simulations on 2D and 3D XY SG, suggest that there is no phase transition in the 2D XY SG without taking into account the chiralities. In these circumstances experimental studies on XY random magnetic systems are clearly needed.

There has been little experiment on short-ranged XY SG. Katsumata *et al.*¹¹ have found that a random mixture of the quasi-2D antiferromagnet (Rb_2MnCl_4) and ferromagnet (Rb_2CrCl_4) exhibits SG behavior in the intermediate concentration region. Independently, Kohles *et al.*¹² have observed SG behavior in the same system. It turned out that the mixed crystal $\text{Rb}_2\text{Mn}_{1-x}\text{Cr}_x\text{Cl}_4$ is a typical example of a 2D XY SG as described below. In this paper we report full details of magnetic, as well as neutron scattering studies, made on the $\text{Rb}_2\text{Mn}_{1-x}\text{Cr}_x\text{Cl}_4$ system and discuss the experimental results in the light of current theories.

The format of this paper is as follows. In Sec. II we present the relevant background information and details. The experimental results are given in Sec. III. A discussion and conclusions are given in Sec. IV.

TABLE I. The lattice parameters, transition temperatures, and parameters of the spin Hamiltonians of Rb_2MnCl_4 and Rb_2CrCl_4 .

	Rb_2MnCl_4	Rb_2CrCl_4
Lattice parameters (\AA)	$a=5.05$ $c=16.18$	$a=5.14$ $c=15.77$
Transition temperature (K)	$T_N=55$	$T_C=52.4$
Spin direction	c axis	c plane ([110])
Effective spin	$\frac{5}{2}$	2
g value	2.00	2.1
Parameters of the Hamiltonian (cm^{-1})	$J=-4.7$ $g\mu_B H_A=0.14$	$J=5.25$ $D=0.737$ $P=0.0855$

II. PRELIMINARY DETAILS

A. Crystal and magnetic properties of Rb_2MnCl_4 and Rb_2CrCl_4

The compound Rb_2MnCl_4 (Ref. 13) has the K_2NiF_4 crystal structure shown in Fig. 2. The crystal has a layered structure. Each successive MCl_2 (where M stands for magnetic atom) layer is separated by two RbCl planes. The crystal structure of Rb_2CrCl_4 is predominantly of the K_2NiF_4 type.¹⁴ There is a small antiferro-distortive displacement of the Cl^- ions within the (001) plane to give two CrCl_6 units with their principal axes of elongation, respectively, along the [100] and [010] axes.¹⁵ The lattice parameters of Rb_2MnCl_4 (Ref. 13) and Rb_2CrCl_4 (Refs. 14 and 15) are shown in Table I. They differ from each other only slightly. Thus, we expect

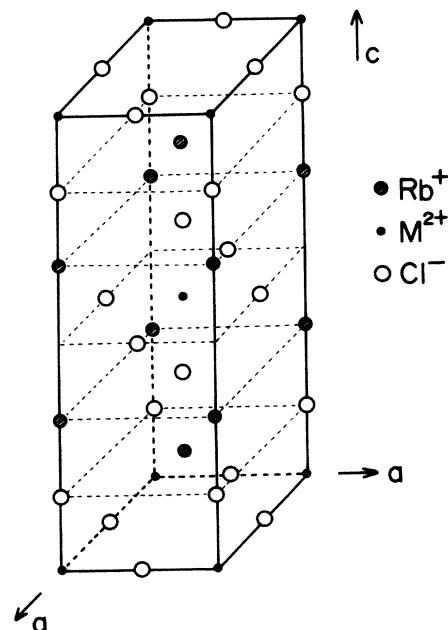


FIG. 2. Crystal structure of Rb_2MCl_4 ($M=\text{Mn}^{2+}$ or Cr^{2+}).

that Rb_2MnCl_4 and Rb_2CrCl_4 make a good solid solution over the whole range of concentration.

Manganese(II) ion has a $(3d)^5$ electron configuration, and the ground state is 6S . Since the ground orbital state of Mn^{2+} is a singlet, it is not affected by mixing with Rb_2CrCl_4 . The main origin of the anisotropy energy in Rb_2MnCl_4 comes from the magnetic dipole-dipole interaction between the Mn^{2+} spins. Chromium(II) ion has a $(3d)^4$ electron configuration and the ground state is 5D . The ground-state orbital wave function of Cr^{2+} in a tetragonal field is either $\xi^2-\eta^2$ or $3r^2-\xi^2$ type. Since the Cl^- octahedron in Rb_2CrCl_4 elongates alternatively along the [100] and [010] directions, the $\xi^2-\eta^2$ state has the lowest energy, where the ξ axis is parallel to the direction of the elongation and the η axis to the c axis of the crystal. Because the Cr^{2+} orbital ground state in Rb_2CrCl_4 is a singlet, it is not affected by mixing with Rb_2MnCl_4 . The anisotropy energy of the Cr^{2+} in Rb_2CrCl_4 comes from the single-ion type, due to the crystal field levels.

From the neutron scattering study,¹⁶ Rb_2MnCl_4 is a 2D antiferromagnet in the temperature range $55 \text{ K} < T < 180 \text{ K}$. Below 55 K (T_N), this compound exhibits a long-range antiferromagnetic ordering. The Mn^{2+} spins in the c plane point antiparallel to their neighboring spins and parallel to the spins on the next-nearest-neighbor planes. The spin easy axis in the antiferromagnetic phase is parallel to the c axis. Since the net exchange field acting on the spins in a plane from the spins on the nearest planes is zero in the ordered phase, a very weak exchange interaction between planes is invoked to determine the relative orientation of the spins on neighboring planes. The spin Hamiltonian in Rb_2MnCl_4 may be written as

$$\mathcal{H} = -2J \sum_{i,j} \mathbf{S}_i \cdot \mathbf{S}_j - g\mu_B H_A \sum_i S_i^z, \quad (1)$$

where J is the in-plane isotropic exchange interaction constant, g the g value along the z axis, μ_B the Bohr magneton, H_A the anisotropy field, and z is parallel to the c axis of the crystal. The parameters of the Hamiltonian have been determined from the antiferromagnetic resonance experiments¹⁷ and are given in Table I.

The neutron experiments¹⁸⁻²⁰ show that Rb_2CrCl_4 is a typical example of a 2D easy-plane ferromagnet. The ratio of the in plane and between planes exchange constants is ~ 0.0003 . The compound Rb_2CrCl_4 exhibits 3D ferromagnetic ordering below 52.4 K (T_C). As is described above, the CrCl_6 units elongate alternatively along the [100] and [010] axes, which correspond to the easy axes in the (001) plane of the sublattices 1 and 2. Due to the strong ferromagnetic exchange interaction spins on the sublattices 1 and 2 point almost parallel to the [110] direction. Hutchings *et al.*¹⁸ used the following spin Hamiltonian to analyze the spin-wave spectra of Rb_2CrCl_4 :

$$\mathcal{H} = -\tilde{J} \sum_{i,j} \mathbf{S}_{i1} \cdot \mathbf{S}_{j2} - \tilde{P} \sum_i (S_{i1a}^2 + S_{i2b}^2) + \tilde{D} \sum_i (S_{i1c}^2 + S_{i2c}^2), \quad (2)$$

where \tilde{J} is the isotropic ferromagnetic exchange constant in the c plane, \tilde{P} and \tilde{D} are single ion anisotropy constants, suffixes 1 and 2 refer to the two sublattices, and a , b , and c to the crystal axes. If we neglect the small canting of the spins on the sublattices 1 and 2, the Hamiltonian (2) reduces to¹⁸

$$\mathcal{H}' = -J \sum_{i,j} \mathbf{S}_i \cdot \mathbf{S}_j + D \sum_i (S_i^x)^2 - P \sum_i (S_i^z)^2, \quad (2')$$

where x is along the c axis and z is parallel to the [110] direction. The values of the parameters of the Hamiltonian [Eq. (2')] obtained from the neutron experiment¹⁸ are given in Table I. Dang *et al.*²¹ estimated the anisotropy field in the a - b plane to be about 1.5 kOe from their nuclear-magnetic-resonance (NMR) study. Using $g=2.1$,²² the in plane anisotropy energy is 0.15 cm^{-1} , which is larger than that obtained in the neutron experiment.¹⁸

B. Experimental details

Several papers have been published²³⁻²⁵ about the best way to grow single crystals of Rb_2MnCl_4 , Rb_2CrCl_4 , and their solid solutions. We have grown the single crystals of $\text{Rb}_2\text{Mn}_{1-x}\text{Cr}_x\text{Cl}_4$ used in the present study by the following method. The starting materials were MnCl_2 , CrCl_2 , and RbCl . Powders of MnCl_2 were obtained by a direct reaction of Mn metal (Johnson Matthey, Specpure) with HCl gas (Seitetsu Chemicals, EG grade). Powders of CrCl_2 and RbCl (Suprapur) were supplied from Merck. The single crystals of Rb_2MnCl_4 were grown from a melt of RbCl and MnCl_2 , the starting ratio of which was slightly offset from the stoichiometric one. The single crystals of Rb_2CrCl_4 were grown similarly. The single crystals of Rb_2MnCl_4 and Rb_2CrCl_4 so obtained were crushed into powders and packed into a quartz ampoule with $1-x$ and x molar ratio. Because these materials are very hygroscopic, all handling was carried out in a glove box filled with dry N_2 gas. The material was purified several times under HCl gas and sealed at the vacuum of 10^{-6} Torr. Then it was set in a vertical furnace, the bottom of which was placed 10 cm below the center of the furnace where the temperature gradient is maximum. The temperature of the furnace was kept above the melting point of $\text{Rb}_2\text{Mn}_{1-x}\text{Cr}_x\text{Cl}_4$ for one day and then lowered slowly. Neither the furnace nor the ampoule was moved. We found that this method is better than the others for obtaining single crystals of the mixture with small concentration gradient. Good single crystals of $\text{Rb}_2\text{Mn}_{1-x}\text{Cr}_x\text{Cl}_4$ as large as $10 \times 10 \times 20 \text{ mm}^3$ could be cleaved from the boules. X-ray and neutron diffraction measurements showed that the single crystals were of reasonable quality. The concentrations (x) of the mixed crystals used in most of the susceptibility and magnetization measurements were determined by means of rf inductively coupled plasma atomic emission spectroscopy. The x values given with only one figure in some of the susceptibility, electron spin resonance (ESR), and neutron scattering results are the starting compositions.

The ac susceptibility (χ) was measured with the fully

computerized apparatus reported earlier.²⁶ The sample was cooled from room temperature to 4.2 K under zero external magnetic field and the ac χ was measured under zero field by slowly increasing the temperature. The magnetization measurements were made with the magnetometer described earlier.²⁶ In order to avoid remanence fields which could be present in a superconducting magnet, we have used a solenoid coil wound with Cu wire. No attempt was made to reduce the Earth's magnetic field in the ac χ and magnetization measurements.

The ESR experiments at millimeter and submillimeter wavelengths were performed with the spectrometer described earlier.²⁷ The microwave sources consist of several Carcinotrons²⁸ made by Thomson-CSF.

The neutron scattering experiments were carried out using a triple-axis spectrometer at the Brookhaven high flux beam reactor. The spectrometer was operated with an incident neutron energy of 14.7 meV obtained from the (002) reflection of a pyrolytic graphite monochromator. The sample was mounted in a helium cryostat with the c axis either vertical or horizontal.

C. Characterization of $\text{Rb}_2\text{Mn}_{1-x}\text{Cr}_x\text{Cl}_4$

We have characterized some of the $\text{Rb}_2\text{Mn}_{1-x}\text{Cr}_x\text{Cl}_4$ single crystals grown for this study from ac χ and ESR measurements. In Fig. 3 we show temperature dependencies of χ along the c axis (χ_{\parallel}) and c plane (χ_{\perp}) of Rb_2CrCl_4 . Upon lowering the temperature, χ_{\perp} increases dramatically around 55 K and shows a plateau below about 53 K. On the other hand, χ_{\parallel} is sharply peaked at 52.8 K. The magnitude of χ_{\perp} is about 100 times larger than that of χ_{\parallel} . The anisotropy of χ in the c plane is very small. The susceptibility (χ_{obs}) of a ferromagnet observed in an experiment in the presence of a demag-

netizing field is related to the intrinsic susceptibility (χ_{int}) by,

$$\chi_{\text{obs}} = 1/(N + 1/\chi_{\text{int}}), \quad (3)$$

where N is the demagnetizing factor. Below T_C , χ_{int} diverges and consequently χ_{obs} is given by $1/N$. We estimated the value of $1/N$ of our sample using the demagnetizing factor given by Osborn,²⁹ and obtained a reasonable agreement with the observation. Thus, the susceptibility measurement confirms that Rb_2CrCl_4 is a good example of a planar ferromagnet. The temperature at which χ_{\parallel} is sharply peaked corresponds to the Curie temperature (T_C). This value of T_C (52.8 K) agrees well with that¹⁸ reported. The behavior of χ_{\parallel} below T_C is explained as follows. Since Rb_2CrCl_4 is a planar magnet, we introduce an effective anisotropy field (H_a) which confines the spins into the c plane. From the balance of torque we have,

$$MH \sin\theta = MH_a \cos\theta, \quad (4)$$

where M is the magnetization, H the external magnetic field along the c axis, and θ is the angle that \mathbf{M} makes with \mathbf{H} . By definition χ_{\parallel} is given by

$$\chi_{\parallel} = \lim_{H \rightarrow 0} M(\cos\theta)/H. \quad (5)$$

Using anisotropy constant (K), H_a is expressed as $H_a = K/M$. The temperature dependence of K is given by $K \sim [M(T)]^n$ with $n \approx 3$.³⁰ Hence, from Eqs. (4) and (5),

$$\chi_{\parallel}(T) \sim [M(T)]^{2-n} \sim [M(T)]^{-1}. \quad (6)$$

The temperature dependence of $M(T)$ is such that $M(T)$ is zero at T_C and increases with decreasing temperature slightly slower than the $S=2$ Brillouin curve.³¹ Thus, $\chi_{\parallel}(T)$ diverges at T_C and then decreases with lowering temperature below T_C .

We have made ESR measurements on Mn-rich samples of $\text{Rb}_2\text{Mn}_{1-x}\text{Cr}_x\text{Cl}_4$ to characterize their magnetic anisotropy. As is described in Sec. II A, Rb_2MnCl_4 is an antiferromagnet with uniaxial anisotropy parallel to the c axis and Rb_2CrCl_4 is a planar ferromagnet with the easy plane perpendicular to the c axis. Therefore, there is a competition^{26,32-37} between the uniaxial and planar anisotropies together with the competition between the antiferromagnetic and ferromagnetic exchange interactions in the mixed system. Since the anisotropy energy of Mn^{2+} spin is much weaker than that of Cr^{2+} spin, we expect that even a small amount of Cr^{2+} atoms changes the uniaxial anisotropy to a planar one. ESR is one of the best methods to characterize spin anisotropy at a microscopic level. Figure 4 shows the result of ESR measurements made on Rb_2MnCl_4 . The frequency (ν) versus external magnetic field (H_0) relation of the resonance points is well described by the following equation for the antiferromagnetic resonance (AFMR) with uniaxial anisotropy,^{38,39}

$$\omega/\gamma = (2H_E H_A)^{1/2} - H_0, \quad (7)$$

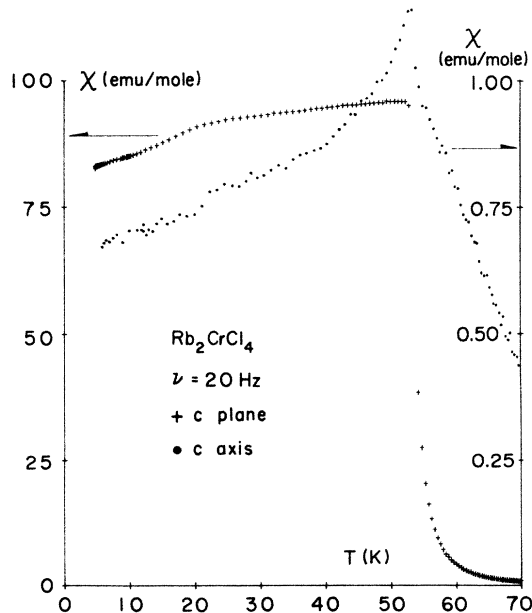


FIG. 3. Temperature dependencies of the ac susceptibilities along the c axis and in the c plane of Rb_2CrCl_4 single crystal.

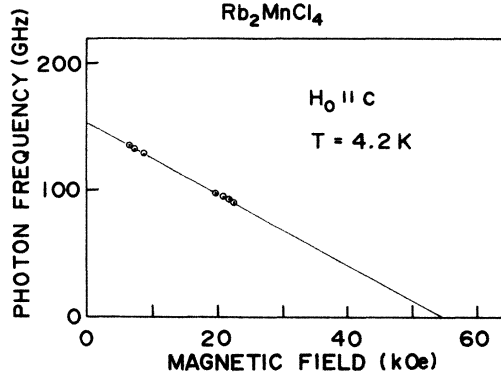


FIG. 4. Frequency vs external magnetic field relation for the antiferromagnetic resonance in Rb_2MnCl_4 obtained at $T=4.2$ K. The external field is applied along the c axis.

where $\omega=2\pi\nu$, $\gamma\equiv g\mu_B/\hbar$, and H_E is the antiferromagnetic exchange field. In Fig. 5 we show the result of ESR experiments on $\text{Rb}_2\text{Mn}_{0.9}\text{Cr}_{0.1}\text{Cl}_4$ sample. We have two resonance branches, the intensities of which are very different from each other. The stronger one corresponds to the AFMR as discussed below. The ν versus H_0 relation of the weaker resonance is expressed by the following equation of a paramagnetic resonance (PMR):

$$\omega/\gamma = H_0. \quad (8)$$

The ν versus H_0 relation of the AFMR in the $x=0.1$ sample is qualitatively different from that of pure Rb_2MnCl_4 . The ν versus H_0 relation of Fig. 5 is well described by the equation

$$\omega/\gamma = (C_1 + H_0^2)^{1/2}. \quad (9)$$

Equation (9) gives the AFMR frequency in the case when the sublattice magnetizations point along the easy axis and H_0 is applied perpendicular both to the easy and hard axes.^{38,39} Thus, the present result shows clearly that the spins in the $x=0.1$ sample lie already in the c

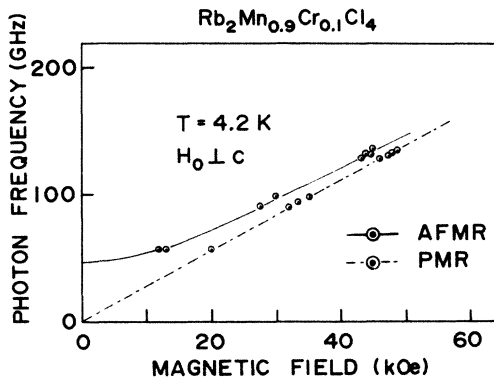


FIG. 5. Frequency vs magnetic field relations for the resonance points in $x=0.1$ sample obtained at $T=4.2$ K. The external field is applied in the c plane. The solid curve is the theoretical one for the antiferromagnetic resonance (AFMR) discussed in the text. The dashed line is for the paramagnetic resonance (PMR).

plane. We present in Fig. 6 ESR data obtained in $\text{Rb}_2\text{Mn}_{0.7}\text{Cr}_{0.3}\text{Cl}_4$. In this sample we have also two resonance branches as in the $x=0.1$ sample. The behavior of the AFMR branch in the $x=0.3$ sample differs from that of the $x=0.1$ sample in that the former deviates from the PMR branch, while the latter tends to it as H_0 increases. Due to frustration effects, the antiferromagnetic exchange field H_E becomes small with increasing x , while the out of plane anisotropy field (H_{A2}) becomes large with x because the planar anisotropy of the Cr spin has already overcome the uniaxial anisotropy of the Mn spin. In the case when $H_{A2}\sim H_E$, we have to retain many terms^{40,41} in the AFMR theory which can be neglected in a usual antiferromagnet. The AFMR frequency is given by

$$\begin{aligned} \omega/\gamma = \{ & H_{A1}(2H_E + H_{A2}) + H_0^2 \\ & + [(-H_{A1}H_{A2} + 2H_EH_{A2} - 6H_{A1}H_E \\ & - H_{A1}^2)/(2H_E + H_{A1})^2]H_0^2\}^{1/2}, \quad (10) \end{aligned}$$

where H_{A1} is the in plane anisotropy field. Experimentally, the resonance frequency extrapolated to $H_0=0$ is very small. Therefore, we may neglect H_{A1} in Eq. (10). Then, Eq. (10) reduces to

$$\omega/\gamma \simeq H_0(1 + H_{A2}/2H_E)^{1/2}. \quad (11)$$

By comparing Eq. (11) with the experiment, we have $H_{A2}/2H_E \simeq 0.7$. From the ESR experiments we can conclude that the magnetic anisotropy in the mixed crystal $\text{Rb}_2\text{Mn}_{1-x}\text{Cr}_x\text{Cl}_4$ is of planar type in the concentration region $0.1 \lesssim x \leq 1$, and that the antiferromagnetic exchange field becomes small with increasing x due to frustration effects. The latter conclusion does not necessarily mean a decrease of the $\text{Mn}^{2+}-\text{Mn}^{2+}$ antiferromagnetic interaction at each site, since we are measuring only the uniform mode in the ESR experiments. Thus, $\text{Rb}_2\text{Mn}_{1-x}\text{Cr}_x\text{Cl}_4$ is a typical example of a 2D XY random magnet with competing exchange interactions.

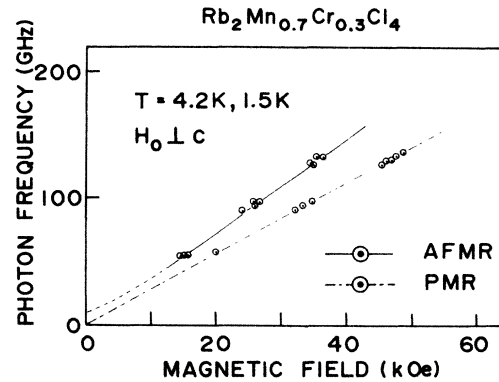


FIG. 6. Magnetic field dependencies of the resonance frequencies in $x=0.3$ sample obtained at $T=4.2$ and 1.5 K. The external field is applied in the c plane. The solid curve is the theoretical one for the antiferromagnetic resonance (AFMR) discussed in the text. The dashed line is for the paramagnetic resonance (PMR).

III. EXPERIMENTAL RESULTS

A. Magnetic measurements

Figures 7(a)–7(d) show the temperature dependencies of χ_{\parallel} and χ_{\perp} of $\text{Rb}_2\text{Mn}_{1-x}\text{Cr}_x\text{Cl}_4$ obtained in the Mn-rich concentration region. The result on the $x=0.03$ sample [Fig. 7(a)] is reminiscent of the susceptibility in a uniaxial antiferromagnet; the parallel susceptibility decreases below T_N , while the perpendicular susceptibility is less temperature dependent. Thus, the $x=0.03$ sample is predominantly a uniaxial antiferromagnet. The susceptibility measurement on $x=0.05$ crystal [Fig. 7(b)] shows that the sample is no longer a uniaxial antiferromagnet. There is an indication of a phase transition in χ_{\parallel} around 28 K. This transition may be related to the

competition of the anisotropies described in Sec. II C. When we increased the Cr concentration further, no indication of phase transition was observed in the susceptibility measurements [Figs. 7(c) and 7(d)].

We show in Fig. 8(a) the temperature dependencies of χ_{\parallel} and χ_{\perp} obtained in the $x=0.34$ sample. In this concentration, χ_{\perp} shows a cusp at 5.6 K (T_{SG}). Also, χ_{\parallel} shows a cusp at the temperature slightly lower than T_{SG} . The susceptibility is anisotropic; χ_{\perp} is about 10 times larger than χ_{\parallel} . Figure 8(b) shows the frequency dependence of χ_{\parallel} obtained in the $x=0.34$ sample. The temperature at which χ_{\perp} shows the cusp increases with increasing frequency of the ac field. The magnitude of χ_{\perp} also depends on the frequency. These behaviors of the ac susceptibility are generally observed in metallic as

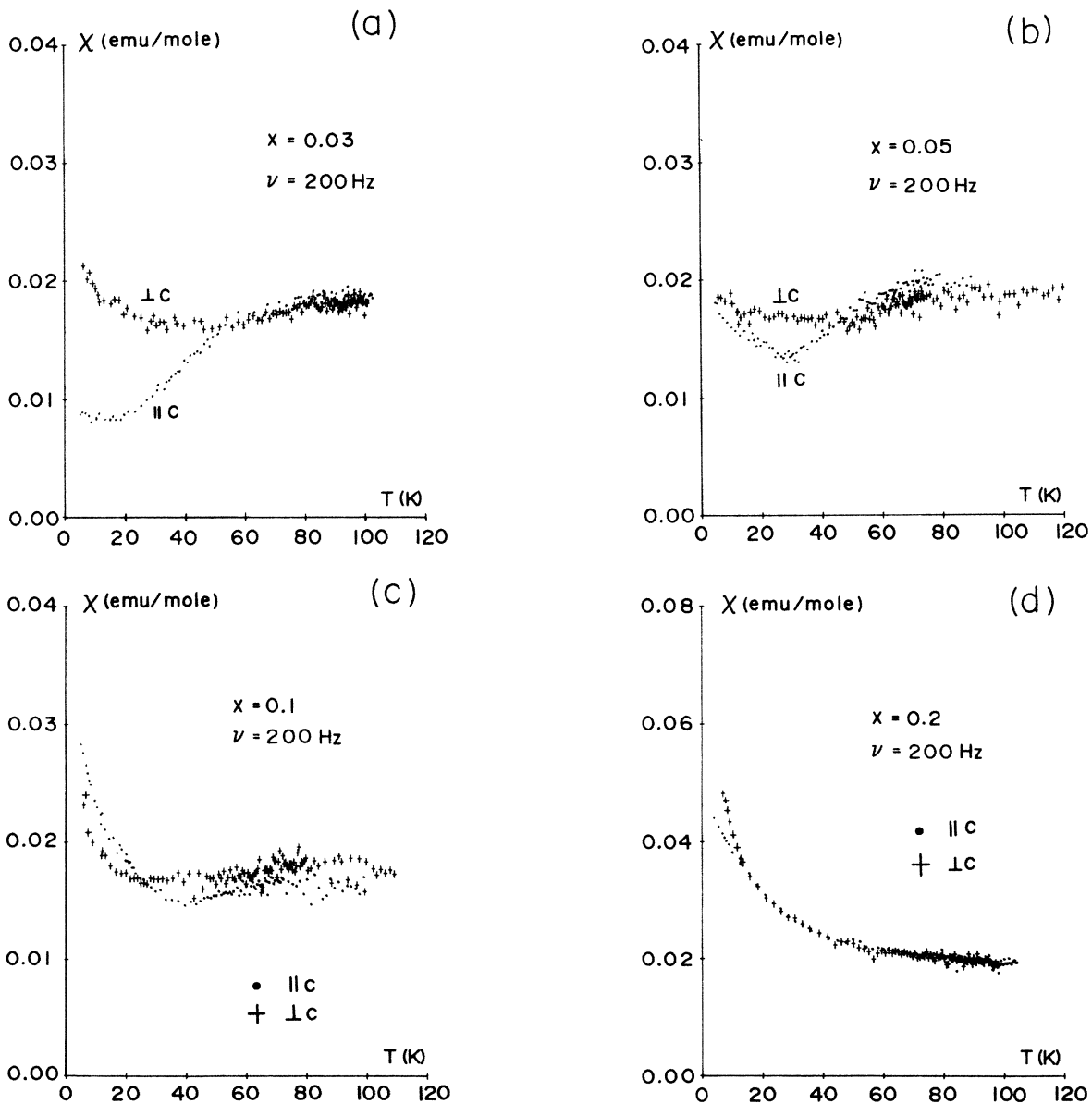


FIG. 7. Temperature dependencies of the ac susceptibilities along the c axis (parallel to c) and in the c plane (perpendicular to c) of $\text{Rb}_2\text{Mn}_{1-x}\text{Cr}_x\text{Cl}_4$ in the Mn-rich concentrations.

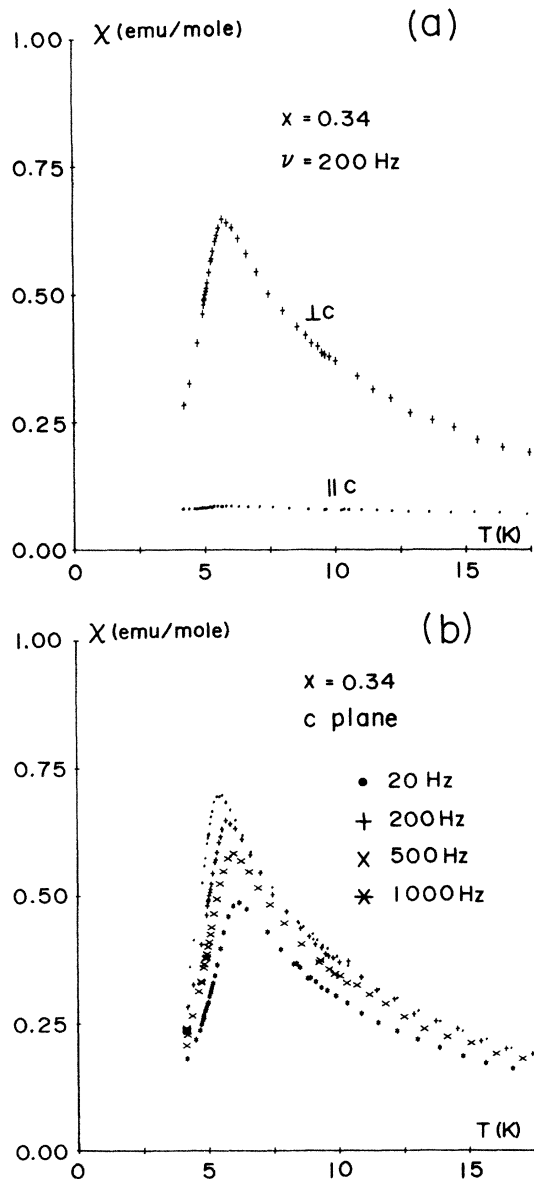


FIG. 8. (a) Temperature dependencies of the ac susceptibilities along the c axis and in the c plane of $x=0.34$ sample. (b) Frequency dependence of the ac susceptibility in the c plane of the $x=0.34$ crystal.

well as insulating spin glasses.⁴² In most cases ac χ does not depend on the measuring frequency above T_{SG} . In our case, χ depends on the frequency in the temperatures $T \lesssim 4T_{SG}$ at the high-frequency region. We show in Fig. 9 the results of magnetization measurements made on the $x=0.4$ crystal under field-cooled (FC) and zero-field-cooled (ZFC) conditions. In the ZFC case, the sample was cooled from room temperature down to 1.5 K in zero external field and a magnetic field of 60 Oe was switched on at 1.5 K. Then, the magnetization was measured in the presence of the magnetic field by slowly increasing the temperature. In the FC case the sample was cooled from room temperature to 1.5 K in the presence of the external field and the magnetization was measured with increasing temperature. The magnetiza-

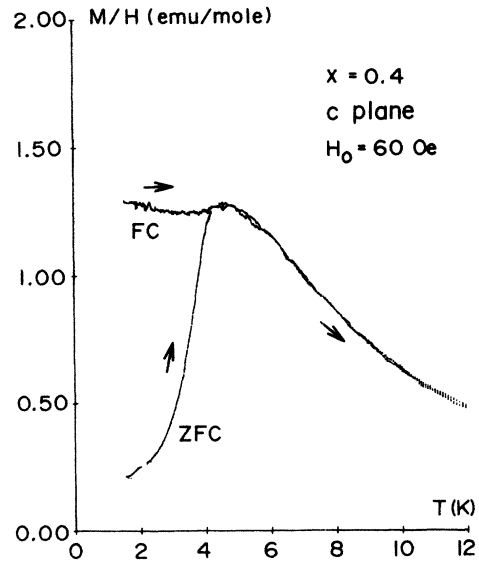


FIG. 9. Temperature dependencies of the zero-field cooled (ZFC) and field cooled (FC) magnetizations in $x=0.4$ sample. The external field is applied in the c plane.

tion is history dependent. This irreversibility of magnetization is commonly seen in SG. From the ac χ and magnetization measurements, we find that $\text{Rb}_2\text{Mn}_{1-x}\text{Cr}_x\text{Cl}_4$ undergoes a PM to SG transition in the intermediate concentration region.

Figures 10(a)–10(d) show the temperature dependencies of ac χ obtained in the Cr-rich concentration region. In these concentrations we see an indication of an RSG transition in χ_{\perp} ; on decreasing temperature χ_{\perp} increases abruptly around T_C and then reaches a plateau. When the temperature is lowered further, χ_{\perp} shows a sharp decrease. The height of the plateau becomes small with decreasing x . As we have used in the susceptibility measurements samples with similar shapes and dimensions, N in Eq. (3) does not differ much from sample to sample. This means that χ_{int} does not diverge below T_C in the ferromagnetic samples rich in Mn atoms. The value of χ_{\perp} is much larger than that of χ_{\parallel} , thus demonstrating that the mixed crystals in these concentrations have a planar anisotropy. The PM-FM transition becomes broad and the value of T_C becomes small as x is decreased from 1. On the other hand, the RSG transition observed at the lower temperature is sharp in the $x=0.50$ sample and becomes broad with increasing x . The disordering transition temperature ($T_{SG} \sim 10$ K) estimated from the inflection point of the χ versus T curve is almost independent of the concentration. In Fig. 11 we show frequency dependencies of χ_{\parallel} and χ_{\perp} obtained in the $x=0.50$ crystal. The susceptibility in the c plane does not depend on the frequency above T_C , while it does depend on the frequency below T_C . The RSG transition becomes broad as the frequency is increased. The susceptibility along the c axis depends on the frequency even above T_C . An indication of the RSG transition is seen in χ_{\parallel} at the same temperature where χ_{\perp} shows a dropoff. Temperature dependencies of ZFC magnetiza-

tions observed in the $x=0.50$ and 0.64 samples are shown, respectively, in Figs. 12(a) and 12(b). The data exhibit a general tendency that the magnetization increases steeply as the temperature is increased from 1.5 K and becomes less temperature dependent above about 4.5 K. This value of T_{SG} is lower than that determined from the ac χ measurements. A careful inspection of Fig. 12(a) shows that T_{SG} estimated from the inflection point of the magnetization versus temperature curve shifts to the low-temperature side with increasing magnetic field and that the magnetization decreases with increasing temperature above T_{SG} at high fields. The FC magnetizations in these samples are almost temperature independent. The behavior of the frequency-dependent χ and the history-dependent magnetization observed at

the FM-SG transition are similar to the ones observed at the PM-SG transition.

B. Neutron scattering

All the reflections reported in this paper are indexed according to the magnetic unit cell^{16,43} of the K_2NiF_4 structure. Figure 13 shows the results of neutron scattering measurements on $x=0.1$ sample. The intensity of the (100) antiferromagnetic reflection begins to increase at 45 K. The critical scattering at (100.385) is peaked at 45 K. Thus, the $x=0.1$ sample shows a long-range antiferromagnetic ordering below this temperature. The intensities of the (100) and (10-0.25) reflections in $x=0.2$ sample were measured. The intensi-

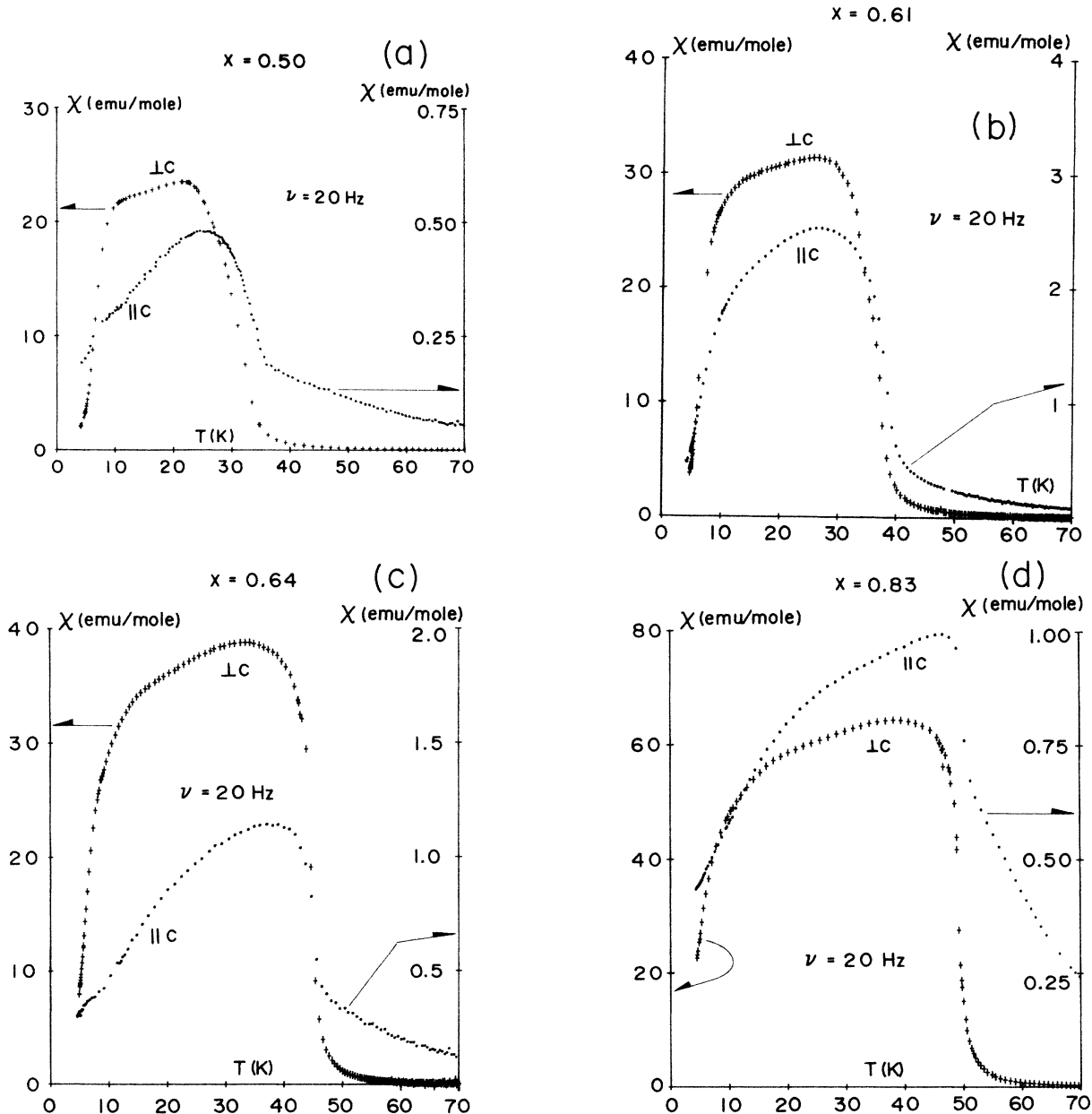


FIG. 10. Temperature dependencies of the ac susceptibilities along the c axis (parallel to c) and in the c plane (perpendicular to c) of $Rb_2Mn_{1-x}Cr_xCl_4$ with $0.50 \leq x$.

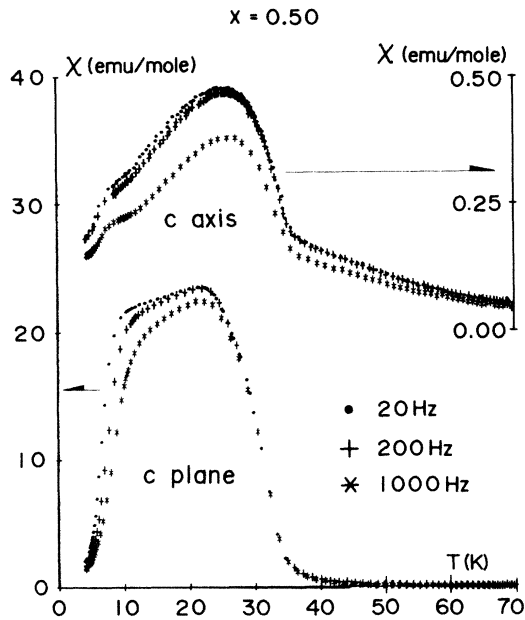


FIG. 11. Frequency dependencies of the ac susceptibilities along the c axis and in the c plane of the $x=0.50$ sample.

ty at the (100) point begins to increase around 30 K and the critical scattering at (10-0.25) is maximum at this temperature. The critical scattering in the $x=0.2$ sample is less pronounced compared to that of the $x=0.1$ sample. Therefore, the antiferromagnetic ordering in the $x=0.2$ sample is smeared.

We now proceed to the Cr-rich concentrations. In this concentration region we have observed scatterings from the ferromagnetic Bragg points and from the antiferromagnetic ones. In the following we discuss only the ferromagnetic scattering. We show in Fig. 14 the temperature dependencies of the (004) and (003.88) reflections obtained in $x=0.6$ sample. The intensity of the (004) reflection begins to increase at 40 K. The critical scattering at (003.88), slightly offset from the Bragg position, shows a peak at 40 K. We see that the ferromagnetic long-range order sets in below 40 K, or at least the ferromagnetic correlation develops considerably below this temperature in the $x=0.6$ sample. Surprisingly, we have no indication of the RSG transition down to 4.7 K. The neutron scattering experiments⁴⁴⁻⁴⁶ on other RSG systems clearly showed a decrease of the inverse correlation length at the RSG transitions. Also, the Bragg intensity exhibited an anomaly there. It is noted that previous neutron observation on $\text{Eu}_x\text{Sr}_{1-x}\text{S}$, where Bragg intensity decreased upon the RSG ordering was made at a subtle concentration region in which the phase boundaries approach to one another. Figure 15 shows the temperature dependences of the intensities at the (004) and (003.9) points observed in $x=0.8$ sample. The Curie temperature of this crystal was determined to be 47 K. We have also no indication of RSG transition in the $x=0.8$ sample down to 1.7 K as in the $x=0.6$ crystal. We have measured the width of the Bragg reflections with a triple-axis configuration. In this

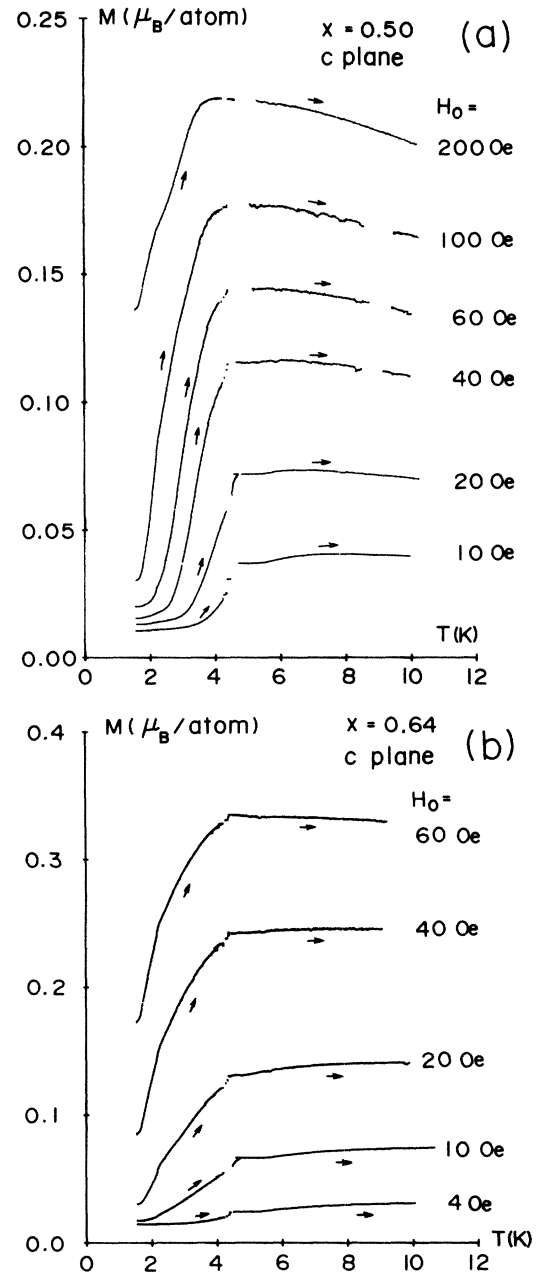


FIG. 12. Temperature dependencies of the zero-field cooled magnetization obtained in the (a) $x=0.50$ and (b) $x=0.64$ crystals. The samples were cooled from room temperature to 1.5 K under zero field and the magnetic fields shown in the figures were switched on at 1.5 K. The measurements were done with slowly increasing the temperature.

case the collimators were changed to all 10'. The longitudinal momentum resolution thus obtained was 0.01 \AA^{-1} [full width at half maximum (FWHM)]. The (004) Bragg reflection in the $x=0.8$ sample was limited by the instrumental resolution below T_C . This means that the correlation length is longer than 400 \AA .

In order to find evidence for the RSG transition from neutron scattering experiments, we carried out a very-high-statistics measurement on the $x=0.5$ crystal with a triple-axis configuration; the results are shown in Fig.

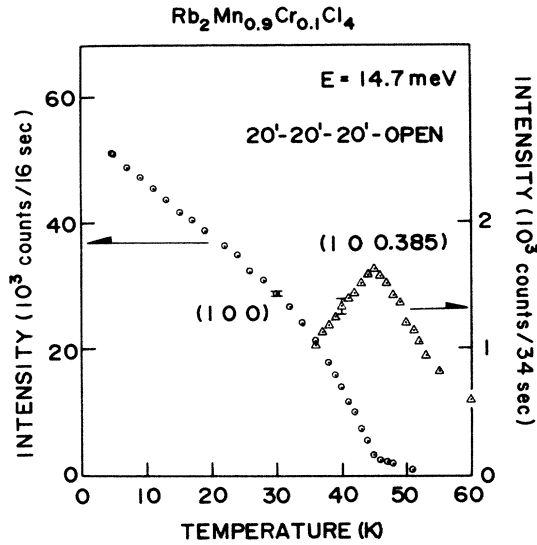


FIG. 13. Temperature dependencies of the intensity of the (100) and of the critical scattering at (100.385) obtained for the $x=0.1$ single crystal. The data points are the average over five to ten measurements, and the typical error bars are indicated.

16. When the sample is cooled from a high temperature ($\gg T_C$) to 4.7 K in zero external magnetic field, and the temperature is increased from there, the intensity at the (003.88) point shows a minimum at about 10 K. The peak in the temperature dependence of the (003.88) intensity at about 33 K represents the critical scattering at the PM-FM transition. When the sample is cooled from

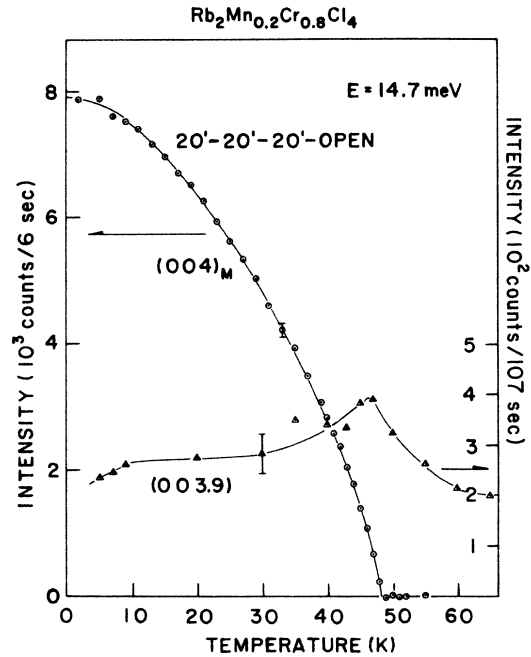


FIG. 15. Temperature dependencies of the intensity of the (004) reflection and of the critical scattering at (003.9) obtained for $x=0.8$ single crystal. The intensity of the (004) nuclear reflection has been subtracted. The data points are the average over five to ten measurements, and typical error bars are indicated.

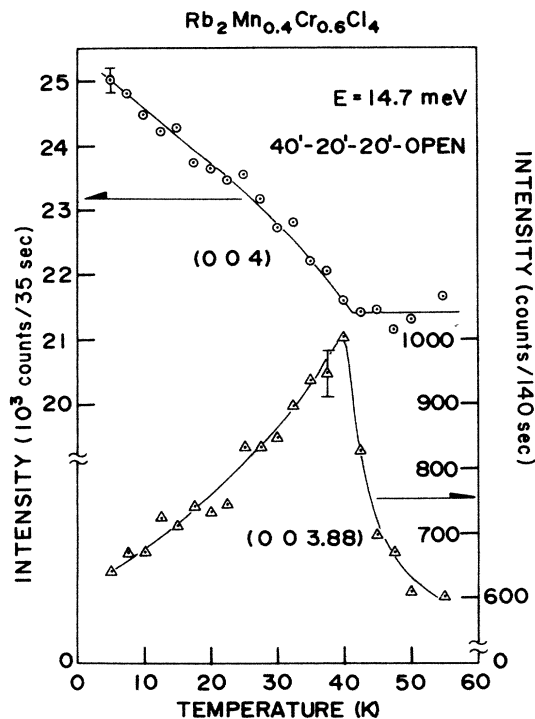


FIG. 14. The intensity of the (004) reflection and the critical scattering at (003.88) obtained in $x=0.6$ single crystal are shown as functions of temperature.

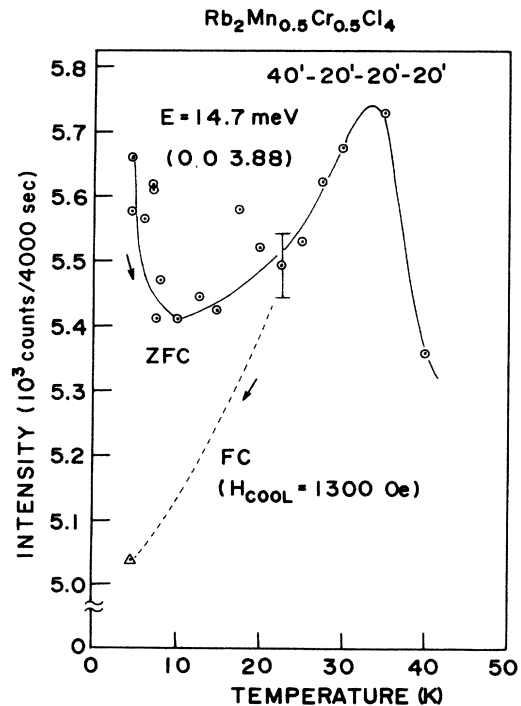


FIG. 16. Temperature dependencies of the intensity at the (003.88) point obtained for the $x=0.5$ single crystal under zero-field cooled (ZFC) and field cooled (FC) conditions.

a high temperature to 4.7 K in the presence of the external magnetic field applied in the c plane, the intensity of the (003.88) reflection at 4.7 K is considerably smaller than that of the ZFC case. These results show that the spin system in this concentration becomes less ordered below 10 K in the ZFC condition, and that the ferromagnetic ordering persists down to the lowest temperature in the FC case. The temperature at which the (003.88) intensity is minimum, agrees well with the RSG transition temperature determined from the susceptibility measurement.

C. Phase diagram

The concentration (x) versus transition temperature (T) phase diagram of $\text{Rb}_2\text{Mn}_{1-x}\text{Cr}_x\text{Cl}_4$ determined from the ac χ and neutron scattering experiments is shown in Fig. 17. The transition temperatures obtained in the two measurements agree well with each other. While the transition temperature from the PM to FM phase varies only slightly with x for $0.8 < x < 1.0$, it decreases sharply as the Mn concentration is increased further; the RSG transition temperature does not go to zero. Instead the transition becomes broad and disappears with decreasing Mn concentration. In the intermediate concentration region, we see a transition from the PM to SG. The mixed system with the Mn-rich concentrations exhibit antiferromagnetism. The transition temperature from the PM to antiferromagnetic (AF) phase rapidly decreases with increasing Cr concentration. This variation with the Cr concentration takes place much faster than the corresponding decrease of the PM to FM transition temperature. The boundary between the PM and AF phase seems to be smeared when the Cr concentration is increased above ~ 0.2 . The x - T phase diagram of $\text{Rb}_2\text{Mn}_{1-x}\text{Cr}_x\text{Cl}_4$ has been reported by Münnighoff *et al.*⁴⁷ Qualitatively, the phase diagram obtained by Münnighoff *et al.* agrees with ours. However, the two phase diagrams differ with each other in the following

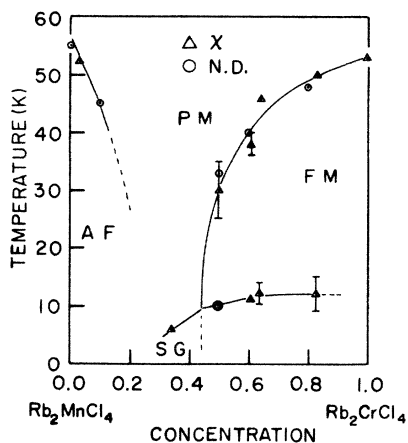


FIG. 17. Concentration versus transition temperature phase diagram of $\text{Rb}_2\text{Mn}_{1-x}\text{Cr}_x\text{Cl}_4$ in zero magnetic field obtained from the ac susceptibility (Δ) and neutron scattering (\circ) measurements. P, paramagnetic phase; AF, antiferromagnetic phase; SG, spin-glass; F, ferromagnetic phase.

points: firstly, the PM to FM transition temperature in Ref. 47 decreases with x much faster than ours; secondly, no phase boundary is given for the PM-SG and FM-SG transitions in the diagram of Münnighoff *et al.*; thirdly, the shape of the PM-AF phase boundary in the two diagrams are different from each other.

IV. DISCUSSION AND CONCLUSIONS

First, we discuss the general features of the x - T phase diagram obtained in this study (Fig. 17). As is described in Sec. III C, the transition temperature from the PM to FM phase varies only slightly with x for $0.8 < x < 1.0$, and it decreases sharply as the Mn concentration is increased further in agreement with the theories.^{48–54} The physical explanation for this behavior is the following. In this site random magnet, we should take at least three kinds of exchange interactions into account: $J_{\text{Cr-Cr}}$ between the ferromagnetic atoms, $J_{\text{Mn-Mn}}$ between the antiferromagnetic atoms, and $J_{\text{Mn-Cr}}$ between the Mn and Cr atoms. When a small number of Mn atoms is embedded into the ferromagnetic matrix, there is little probability of finding pairs of Mn atoms. In this case, we can find a spin configuration for which each spin points in a direction such that the exchange energy is minimized. As the number of antiferromagnetic atoms increases, the probability of finding pairs of these atoms increases. A frustration then occurs when $J_{\text{Mn-Cr}} \neq 0$. Therefore, the Curie temperature changes very little when the concentration of Mn atoms is small, but decreases with the concentration in the region for which the frustration effect is appreciable. The transition temperature from the PM to AF phase rapidly decreases with increasing Cr concentration. This variation with Cr concentration takes place much faster than the corresponding decrease of the PM to FM transition temperature. This is interpreted as a result of the competition^{32–37} of the uniaxial anisotropy of Rb_2MnCl_4 with the planar anisotropy of Rb_2CrCl_4 which lowers the Néel temperature together with the frustration effect. As explained in Sec. III C, our phase diagram is quantitatively different from that reported by Münnighoff *et al.*⁴⁷ We believe that the difference is due to the different ways of determining the concentrations. We have chemically analyzed the crystals used in the present experiments. In some cases we have not chemically checked the crystals and used the starting compositions (given with only one figure in this paper). It turned out that in most cases, the starting compositions were close to the chemically analyzed concentrations. On the other hand, Münnighoff *et al.*⁴⁷ determined the concentrations by structural analysis. The magnetic phase diagram of a similar system $\text{K}_2\text{Cu}_c\text{Mn}_{1-c}\text{F}_4$ has been reported by Kimishima *et al.*⁵⁵ The concentration regions for which the AF and F phases exist in $\text{K}_2\text{Cu}_c\text{Mn}_{1-c}\text{F}_4$ are largely different from those in $\text{Rb}_2\text{Mn}_{1-x}\text{Cr}_x\text{Cl}_4$. Kimishima *et al.*⁵⁵ suggest that the Cu^{2+} atoms in $\text{K}_2\text{Cu}_c\text{Mn}_{1-c}\text{F}_4$ behave as non-magnetic impurities in the AF region. This behavior may be related to the fact⁵⁶ that the cooperative Jahn-Teller distortion disappears below $x \sim 0.4$ in isomorphous $\text{K}_2\text{Cu}_x\text{Zn}_{1-x}\text{F}_4$. A theoretical x - T phase diagram

which takes into account the effects of a cooperative Jahn-Teller distortion has been reported.⁵⁷

Next, we discuss the PM to SG transition observed in the intermediate concentration region of $\text{Rb}_2\text{Mn}_{1-x}\text{Cr}_x\text{Cl}_4$. Experimentally, we have observed clearly the SG behavior; the appearance of a cusp in the temperature dependence of the ac χ [Fig. 8(a)], the frequency-dependent ac χ [Fig. 8(b)], and the irreversibility of the magnetization (Fig. 9). Kawamura and Tanemura⁸ suggest that the uniform χ in the 2D XY SG system does not show any anomaly at T_{SG} in the thermodynamic limit, and that the chiral SG order parameter ($q_{\kappa}^{(2)}$) given by

$$q_{\kappa}^{(2)} = \left[(1/N^2) \sum_{\alpha,\beta} \langle \kappa_{\alpha}\kappa_{\beta} \rangle^2 \right]_J, \quad (12)$$

becomes finite below T_{SG} . In Eq. (12) $\langle \rangle$ means a thermal average for a given bond distribution $\{J_{ij}\}$ and $[\]_J$ means a configurational average. The value of T_{SG} of our sample determined from the ac χ measurement becomes small with lowering frequency. This is consistent with the result of Kawamura and Tanemura. It would be very interesting if we could measure the chiral SG order parameter experimentally.

Finally, we discuss the RSG transition observed in the Cr-rich concentration region. Several papers^{9,58-61} have been published concerning the theory and model on RSG transitions. Sherrington and Kirkpatrick⁵⁸ discussed the infinite-ranged Ising SG model and Gabay and Toulouse⁵⁹ extended the theory to vector spin systems. Although they have found RSG behaviors, the theories are not directly applicable to our insulating SG system where the interaction is short ranged. The model for the RSG transition proposed by Aeppli *et al.*⁶⁰ is based on the random-field effect.⁶² The random-field effect is realized in a random Ising antiferromagnet in the presence of an external magnetic field.⁶³ A number of experiments concerning the random field effect has been published.⁶⁴ These results show that when the samples are cooled in a magnetic field, long-range order is not established at low temperatures, but that long-range order is retained when the crystals are cooled in zero field. It is not immediately clear how the random field in Aeppli's model is affected by the external field. However, it seems to be unlikely in the random-field model of RSG that the long-range order is established in the FC case as found in the present neutron scattering experiment and the neutron depolarization study.⁶⁵ Kawamura and Tanemura⁹ and Saslow and Parker⁶¹ discussed the RSG transition in the same 2D XY random system. Since the mixed crystal $\text{Rb}_2\text{Mn}_{1-x}\text{Cr}_x\text{Cl}_4$ is close to an ideal 2D XY random magnet, we discuss the RSG transition in the context of the theories. Essentially, the results of the two papers seem to be very similar to each other. The important difference between the two theories lies in the nature of the RSG state. Kawamura and Tanemura⁹ claim that the RSG state with low net magnetization is a metastable one, and that a phase close to the ferromagnetic one is realized in thermal equilibri-

um. On the other hand, Saslow and Parker⁶¹ showed that the RSG transition signaled by a sudden change in magnetization takes place in both of the heating and cooling conditions. This suggests that the RSG state with the low magnetization is an equilibrium one. Katsumata *et al.*⁶⁵ have reported the result of the neutron depolarization experiment on $\text{Rb}_2\text{Mn}_{0.48}\text{Cr}_{0.52}\text{Cl}_4$. When the sample is cooled from a high temperature to 2 K in zero magnetic field and the temperature is increased, the polarization (P) of the polarized neutron beam transmitted through the sample decreases up to 10 K. In the temperatures between 10 K and T_C , P is almost temperature independent. Then, P begins to increase around T_C . When the sample is cooled to 2 K under a weak magnetic field, P is much smaller than the corresponding value of the ZFC case. The result of the neutron depolarization experiment was interpreted by a domain model.⁶⁵ In the ZFC case the system is decomposed into domains at low temperatures. In the FC case the long-range order is retained. Kubo *et al.*⁶⁶ performed NMR experiments in the Cr-rich concentration region of $\text{Rb}_2\text{Mn}_{1-x}\text{Cr}_x\text{Cl}_4$. A satellite line was observed together with the main lines in $x=0.8$ sample when it is cooled to 1.7 K in zero field. From the analysis of the satellite line, it is shown that about 80% of the moments are ferromagnetically aligned and the directions of the rest of the moments distribute in the c plane at low temperature. These experimental results are consistent with the Monte Carlo study by Kawamura and Tanemura.⁹ They generated a Monte Carlo snapshot of the spin pattern in the RSG state obtained by quenching the sample from a high temperature in zero field. The spin pattern consists of ferromagnetically aligned regions, which may be called domains and vortices. The vortices are formed around the frustrated plaquette pairs with $(++)$ or $(--)$ chiralities. When the sample is cooled from a high temperature in the presence of a magnetic field, the regions of ferromagnetically aligned spins are much larger than those of the ZFC case. Since there is a small anisotropy in the c plane, and a weak exchange interaction between planes in $\text{Rb}_2\text{Mn}_{1-x}\text{Cr}_x\text{Cl}_4$, the actual spin configuration in the RSG state may be slightly different from that obtained in the Monte Carlo study.

More detailed studies of the RSG transition in $\text{Rb}_2\text{Mn}_{1-x}\text{Cr}_x\text{Cl}_4$ would be quite valuable. Specifically, whether the RSG state with the low net magnetization is a metastable one or not should be explored. We hope that these results will stimulate further theory on the 2D XY SG system.

ACKNOWLEDGMENTS

We would like to thank A. Aharony, D. P. Belenger, R. J. Birgeneau, B. Briat, R.A. Cowley, P. Day, Y. Endoh, R. Geick, K. Hirakawa, the late Y. Ishikawa, H. Kawamura, H. Kubo, F. Matsubara, S. Mitsuda, Y. Miyako, K. Nagata, T. Oguchi, W. Saslow, S. M. Shapiro, G. Shirane, M. Suzuki, H. Takayama, M. Tanimoto, G. Toulouse, Y. Tsunoda, and P. J. Walker for helpful discussions. The work done in Japan was partially support-

ed by a Grant-in-Aid for Scientific Research from the Ministry of Education, Science and Culture. The neutron scattering study was carried out as part of the U.S.-Japan Cooperative Neutron Scattering Program.

Work at Brookhaven National Laboratory was supported by the Division of Materials Sciences, U.S. Department of Energy under Contract No. DE-AC02-76CH00016.

- ¹A. J. Bray, M. A. Moore, and A. P. Young, *Phys. Rev. Lett.* **56**, 2641 (1986).
- ²R. N. Bhatt and A. P. Young, *Phys. Rev. Lett.* **54**, 924 (1985).
- ³A. T. Ogielski and I. Morgenstern, *Phys. Rev. Lett.* **54**, 928 (1985).
- ⁴I. Morgenstern and K. Binder, *Phys. Rev. Lett.* **43**, 1615 (1979).
- ⁵For example, B. W. Morris, S. G. Colborne, M. A. Moore, A. J. Bray, and J. Canisius, *J. Phys. C* **19**, 1157 (1986).
- ⁶G. Toulouse, *Commun. Phys.* **2**, 115 (1977).
- ⁷J. Villain, *J. Phys. C* **10**, 4793 (1977).
- ⁸H. Kawamura and M. Tanemura, *J. Phys. Soc. Jpn.* **54**, 4479 (1985).
- ⁹H. Kawamura and M. Tanemura, *J. Phys. Soc. Jpn.* **55**, 1802 (1986).
- ¹⁰S. Jain and A. P. Young, *J. Phys. C* **19**, 3913 (1986).
- ¹¹K. Katsumata, T. Nire, M. Tanimoto, and H. Yoshizawa, *Phys. Rev. B* **25**, 428 (1982).
- ¹²N. Kohles, H. Theuerkauf, K. Strobel, R. Geick, and W. Treutmann, *J. Phys. C* **15**, L137 (1982).
- ¹³H. J. Seifert and F. W. Koknat, *Z. Anorg. Allg. Chem.* **341**, 269 (1965).
- ¹⁴H. J. Seifert and K. Klatyk, *Z. Anorg. Allg. Chem.* **334**, 113 (1964).
- ¹⁵E. Janke, M. T. Hutchings, P. Day, and P. J. Walker, *J. Phys. C* **16**, 5959 (1983).
- ¹⁶A. Epstein, E. Gurewitz, J. Makovsky, and H. Shaked, *Phys. Rev. B* **2**, 3703 (1970).
- ¹⁷K. Katsumata, J. Tuchendler, and M. Tanimoto, *Solid State Commun.* **50**, 193 (1984).
- ¹⁸M. T. Hutchings, J. Als-Nielsen, P. A. Lindgård, and P. J. Walker, *J. Phys. C* **14**, 5327 (1981).
- ¹⁹M. T. Hutchings, M. J. Fair, P. Day, and P. J. Walker, *J. Phys. C* **9**, L55 (1976).
- ²⁰M. J. Fair, M. T. Hutchings, P. Day, R. Ghosh, and P. J. Walker, *J. Phys. C* **11**, L813 (1978).
- ²¹K. Le Dang, P. Veillet, and P. J. Walker, *J. Phys. C* **10**, 4593 (1977).
- ²²P. Day, E. Janke, T. E. Wood, and D. Woodwark, *J. Phys. C* **12**, L329 (1979).
- ²³J. Makovsky, A. Zolkevit, and Z. H. Kalman, *J. Cryst. Growth*, **11**, 99 (1971).
- ²⁴G. Garton and P. J. Walker, *J. Cryst. Growth* **33**, 61 (1976); **36**, 351 (1976).
- ²⁵P. J. Walker and F. Wondre, *J. Cryst. Growth*, **60**, 155 (1982).
- ²⁶K. Katsumata, J. Tuchendler, and S. Legrand, *Phys. Rev. B* **30**, 1377 (1984).
- ²⁷J. Tuchendler, J. Magariño, and J. P. Renard, *Phys. Rev. B* **20**, 2637 (1979).
- ²⁸Trademark name for backward-wave oscillators.
- ²⁹J. A. Osborn, *Phys. Rev.* **67**, 351 (1945).
- ³⁰J. Kanamori, in *Magnetism*, edited by G. T. Rado and H. Suhl (Academic, New York, 1963), Vol. 1, Chap. 4, pp. 127–203.
- ³¹M. J. Fair, A. K. Gregson, P. Day, and M. T. Hutchings, *Physica* **86-88B**, 657 (1977).
- ³²A. Aharony and S. Fishman, *Phys. Rev. Lett.* **37**, 1587 (1976).
- ³³F. Matsubara and S. Inawashiro, *J. Phys. Soc. Jpn.* **42**, 1529 (1977).
- ³⁴K. Katsumata, M. Kobayashi, T. Sato, and Y. Miyako, *Phys. Rev. B* **19**, 2700 (1979).
- ³⁵Y. Someya, A. Ito, and K. Katsumata, *J. Phys. Soc. Jpn.* **52**, 254 (1983).
- ³⁶P. Wong, P. M. Horn, R. J. Birgeneau, and G. Shirane, *Phys. Rev. B* **27**, 428 (1983).
- ³⁷K. Katsumata, H. Yoshizawa, G. Shirane, and R. J. Birgeneau, *Phys. Rev. B* **31**, 316 (1985).
- ³⁸T. Nagamiya, K. Yosida, and R. Kubo, *Adv. Phys.* **4**, 1 (1955).
- ³⁹S. Foner, in *Magnetism*, Ref. 30, Chap. 9, pp. 383–447.
- ⁴⁰M. Tanimoto, T. Kato, and Y. Yokozawa, *Phys. Lett.* **58A**, 66 (1976).
- ⁴¹H. Yamazaki, E. Soares, H. Panepucci, and Y. Morishige, *J. Phys. Soc. Jpn.* **47**, 1464 (1979).
- ⁴²J. L. Tholence, *Solid State Commun.* **35**, 113 (1980).
- ⁴³R. J. Birgeneau, H. J. Guggenheim, and G. Shirane, *Phys. Rev. B* **1**, 2211 (1970).
- ⁴⁴C. R. Fincher, Jr., S. M. Shapiro, A. H. Palumbo, and R. D. Parks, *Phys. Rev. Lett.* **45**, 474 (1980).
- ⁴⁵S. M. Shapiro, G. Shirane, B. H. Verbeek, G. J. Nieuwenhuys, and J. A. Mydosh, *Solid State Commun.* **36**, 167 (1980).
- ⁴⁶H. Maletta, G. Aeppli, and S. M. Shapiro, *Phys. Rev. Lett.* **48**, 1490 (1982).
- ⁴⁷G. Münnhoff, E. Hellner, W. Treutmann, N. Lehner, and G. Heger, *J. Phys. C* **17**, 1281 (1984).
- ⁴⁸F. Matsubara, *Prog. Theor. Phys.* **52**, 1124 (1974).
- ⁴⁹F. Matsubara and M. Sakata, *Prog. Theor. Phys.* **55**, 672 (1976).
- ⁵⁰Y. Ueno and T. Oguchi, *J. Phys. Soc. Jpn.* **40**, 1513 (1976).
- ⁵¹E. Eggarter and T. P. Eggarter, *Phys. Rev. B* **15**, 2804 (1977).
- ⁵²M. V. Medvedev, *Phys. Status Solidi B* **86**, 109 (1978).
- ⁵³T. Oguchi and Y. Ueno, *J. Phys. Soc. Jpn.* **46**, 729 (1979).
- ⁵⁴S. Fishman and A. Aharony, *Phys. Rev. B* **19**, 3776 (1979).
- ⁵⁵Y. Kimishima, H. Ikeda, A. Furukawa, and H. Nagano, *J. Phys. Soc. Jpn.* **55**, 3574 (1986).
- ⁵⁶Y. Natsume and I. Yamada, *Solid State Commun.* **47**, 839 (1983).
- ⁵⁷F. Matsubara and K. Katsumata, *Solid State Commun.* **49**, 1165 (1984).
- ⁵⁸D. Sherrington and S. Kirkpatrick, *Phys. Rev. Lett.* **35**, 1792 (1975).
- ⁵⁹M. Gabay and G. Toulouse, *Phys. Rev. Lett.* **47**, 201 (1981).
- ⁶⁰G. Aeppli, S. M. Shapiro, R. J. Birgeneau, and H. S. Chen, *Phys. Rev. B* **28**, 5160 (1983).
- ⁶¹W. M. Saslow and G. Parker, *Phys. Rev. Lett.* **56**, 1074 (1986).
- ⁶²For a review see, Y. Imry, *J. Stat. Phys.* **34**, 849 (1984).

⁶³S. Fishman and A. Aharony, *J. Phys. C* **12**, L729 (1979).

⁶⁴For a review see, R. J. Birgeneau, Y. Shapira, G. Shirane, R. A. Cowley, and H. Yoshizawa, *Physica* **137B**, 83 (1986).

⁶⁵K. Katsumata, M. Tanimoto, S. Mitsuda, and Y. Endoh, *J.*

Phys. Soc. Jpn. **53**, 3315 (1984).

⁶⁶H. Kubo, T. Hamasaki, M. Tanimoto, and K. Katsumata, *J. Phys. Soc. Jpn.* **55**, 3301 (1986).